Marine Propeller Noise Propagation within a Shallow Water Environment

MARINE 2021

Giovanni Petris*,[1], Marta Cianferra[1] and Vincenzo Armenio[1]

[1]Department of Engineering and Architecture
University of Trieste
Piazzale Europa, 1, Trieste, Italy

* Corresponding author: Giovanni Petris, giovanni.petris@phd.units.it

ABSTRACT

The present paper contains preliminary results obtained from coupling the Ffowcs-Williams and Hawkings (FW-H) acoustic model with the wave equation solved in the time domain using finite differences. The purpose is to study the propagation of complex noise sources in realistic water basins. The acoustic analogy is used to accurately characterize the source (an isolated marine propeller), whose propagation is then evaluated in an arbitrary domain through the wave equation. Differently from the FW-H equation, which assumes that the pressure disturbance propagates in an open, quiescent, and homogeneous medium, the general wave equation can deal with reflection on the boundaries of the basin and density variations along the water column. As a first experiment, we analyze the propeller signal propagating in a simplified canal, and we show the differences with respect to the open-sea case in terms of sound pressure level.

Keywords: Propeller; FW-H; FDTD; Noise propagation.

NOMENCLATURE

c	Speed of sound [m s^{-1}]
D	Diameter [m]
dB	Decibel [-]
Hz	Hertz [s^{-1}]
$\tilde{p}$	Fluid dynamic pressure [Pa]
p	Acoustic pressure [Pa]
$\mathbf{r}$	Unit radiation vector [m,m,m]
S	Immersed surface [m^2]
t	Time [s]
$\mathbf{v}$	Velocity of the surface S [m s^{-1},m s^{-1},m s^{-1}]
τ	Emission time [s]
ρ	Fluid density [kg m^{-3}]
FDTD	Finite Difference Time Domain
FW-H	Ffowcs-Williams and Hawkings
LES	Large Eddy Simulation
SL	Spectrum Level
SPL	Sound Pressure Level
PML	Perfectly Matched Layer

1 INTRODUCTION

The low-frequency noise generated by a vessel propeller is among the ocean's primary noise pollution sources (Hildebrand, 2009) and cause of danger to the marine fauna (Weilgart, 2007). More stringent regulations (IMO, 2014) on noise emission have led the shipbuilding companies to design silent class ships, to reduce the environmental impact. It turns necessary to develops tools that accurately characterize the noise generated by complex systems and its propagation in a marine environment. Numerical and experimental studies together with field data have revealed that the primary source of noise of vessels is the propeller. Predict how the noise source interacts with the environment is still a difficult task due to the difficulties in performing experiments in the marine environment and to the limits of standard numerical approaches. To date, the most common numerical method, suitable to characterize the noise source, is represented by the Ffowcs-Williams and Hawkings (FW-H) acoustic analogy, which allows to reconstruct the acoustic field by post-processing of hydrodynamics data. In recent years, the need to make the latter very accurate has been highlighted (Iannello 2014; Cianferra 2019), since the coherent structures present in the propeller wake are found to cause strong noise disturbances. Large-Eddy Simulation (LES) represents the best-suited numerical tool to reproduce the fluctuating fluid dynamic field responsible for noise generation since it is the best compromise between effectiveness and efficiency. There are several examples of LES-FW-H coupling in the literature, see among others Broglia *et al.* (2020), Bensow *et al.* (2016), and Keller *et al.* (2018). On the other hand, laboratories for hydroacoustic experiments are developing increasingly sophisticated techniques; see for example Felli *et al.* (2014), where a novel wavelet-based filtering procedure is adopted to investigate the near-field pressure fluctuations on a rudder, at different deflection angles. However, both acoustic analogy and laboratory experiments have inherent limitations, as far as the propagation of noise in realistic environments is concerned. It is not straightforward to obtain measurements on the noise generated by ships in operational conditions. Typically, experiments are opportunistic. Passive measurements are conducted with hydrophones deployed along merchant shipping lanes, such as the analysis performed in the Santa Barbara Channel by McKenna *et al.* (2012). The experiment's conditions, such as the type of ship and the state of the environment, may differ enormously. A better understanding of the interaction between the environment and the source can be gained using numerical simulation. The propagation of a simple acoustic source in a heterogeneous environment may be evaluated by considering the wave equation in the frequency domain, thus solving the Helmholtz equation. Several important applications of this method in the field of marine acoustics are found in the literature, such as the effect of complex morphology seabed on the propagation of a broadband pulse (Sturm, 2005). Over the years, different methods have been proposed to solve different problems since there are no general methods suitable for all conditions (such as the marine environment and type of source). Three different aspects have to be considered: frequency of the source, depth of the water column and the range-dependent environment, as reviewed Etter (2012). The Helmholtz equation has a low computational cost but has some limitations on the source's complexity (especially when complex directivity patterns are present) and on the morphology of the environment. Another option is to solve the wave equation directly in the time domain, using, among the others, the finite difference time domain method (FDTD). This method was neglected in the past due to the high computational cost. It is suitable for low-frequency sources in a limited domain, up to few kilometers. The advantage of this method is the ability to reproduce more complex sources and the environment's variability. The use of this method in the marine environment is still unexplored, and few references are available, such as the work on marine hydrokinetic power devices of Hafla *et al.* (2018). On the other hand, large literature is available on room acoustics, which clearly deals with different types of conditions and applications, but share the same problems of underwater noise research. Using some tools developed for the room acoustic, we try to couple the FW-H method with the FDTD method. The coupling allows the use of the two methods in their domains of applicability and to obtain the noise generated by a marine propeller in a complex environment. The paper is structured as follows. In Section 2, we describe the methods herein implemented, focusing on the coupling between them. In section 3, we report a brief validation of the presented method. In section 4, the results for a marine

environment are discussed. Finally, Section 5 contains concluding remarks.

2 NUMERICAL METHOD

One of the most restricting assumptions of the Ffowcs-Williams and Hawkings analogy is that the noise source, once generated, propagates in a free, homogeneous and quiescent medium. That's the main reason why the FW-H method is suitable to characterize the noise source instead of predicting the noise propagating in a realistic environment. The proposed approach aims at overcoming the FW-H method's limitations by coupling it with a wave equation solver. In particular, by considering a finite-difference wave equation solver, we can consider boundaries and variation of density. Indeed, the acoustic response of a complex marine environment is usually obtained by solving the wave equation in its differential form. The FW-H is used to characterize the noise generated by a marine propeller, which besides has a pronounced directivity pattern. The acoustic pressure obtained through the use of FW-H operates as boundary condition for the Finite-Difference-Time-Domain (FDTD) algorithm. We briefly describe the two methods adopted and the nesting procedure.

2.1 Ffowcs Williams and Hawkings Acoustics Model

At this stage of the study, only the linear terms of the Ffowcs-Williams and Hawkings are considered:

$$4\pi\, p(\mathbf{x},t) \;=\; \frac{\partial}{\partial t}\int_S \left[\frac{\rho_0\ \mathbf{v}\cdot\mathbf{n}}{r}\right]_\tau dS + \frac{1}{c_0}\frac{\partial}{\partial t}\int_S \left[\frac{\tilde{p}\ \mathbf{n}\cdot\mathbf{r}}{r}\right]_\tau dS + \int_S \left[\frac{\tilde{p}\ \mathbf{n}\cdot\mathbf{r}}{r^2}\right]_\tau dS, \tag{1}$$

where c_0 and ρ_0 are the constant speed of sound and density, respectively, $\mathbf{n}$ is the (outward) unit normal vector to the surface element dS, $\mathbf{r}$ is the unit radiation vector and r is its module, $\mathbf{v}$ is the velocity of the surface S, $\tilde{p}$ is the fluid dynamic pressure and τ it the emission time, which in the present case is assumed equal to the observer time t. The FW-H equation (Eq. 1) it applied to the benchmark propeller SVA VP1304 (https://www.sva-potsdam.de/en/potsdam-propeller-test-case-pptc), whose fluid dynamics field was developed through a LES (please refer to Cianferra *et al.* (2019) for the details of both the fluid dynamic simulation and the acoustic analysis of the open-sea propeller).

2.2 Wave Equation and FDTD

The acoustic wave equation (Eq. 2) is solved with the FDTD method to obtain the acoustic pressure propagation in a three-dimensional medium, with variable density and speed of sound:

$$\frac{1}{c(\mathbf{x})^2}\frac{\partial^2 p(\mathbf{x},t)}{\partial t^2} = \rho(\mathbf{x})\nabla^2\left(\frac{1}{\rho(\mathbf{x})}p(\mathbf{x},t)\right) + f(\mathbf{x},t), \tag{2}$$

where c is the speed of sound of the medium, p is the acoustic pressure, ρ is the density of the medium, and $f(\mathbf{x},t)$ is the source term. The equation is solved using a second-order in time and space, explicit scheme. The open-boundary condition, which allows mimicking a boundless domain, is implemented using a Perfectly Matched Layer(PML) (Chern, 2019). We tested the FDTD code (results are not reported here) considering simple sources, like monopole, dipole, and quadrupole sources, for which the analytical solutions are available. We found that the PML is very effective in removing spurious boundary reflections, mostly for homogenous media. However, in the case of a non-homogeneous medium, we observed numerical errors, mostly located at the interface between the two media (the case of a two-density medium was considered). The hard source method is used to implement the propeller signal, meaning that the source pressure, computed through FW-H, is imposed as a boundary condition at specific source nodes of the grid. Therefore in this way, the source function f of Eq. 2

is zero. This method is suitable for low-frequency sources. A main limitation of the FDTD method considered in the present work is related to the forward velocity of the propeller. Indeed, in this case, the source is assumed to be steady and the medium quiescent. However, this condition can be modified, for example, taking into account the advective wave equation. We intend to improve this aspect in future works. However, the approach here considered is still valid due to the small propeller's advance velocity with respect to the speed of sound.

2.3 FW-H and FDTD Coupling

The propeller is placed at the centre (0, 0, 0) of the FDTD domain, which has a constant grid spacing $\Delta x = \Delta y = \Delta z = 4D$, being $D = 0.25\,m$ the propeller diameter. The source acoustic pressure is evaluated with the FW-H method at specific probes: we have chosen a box whose vertices are at $(-6D, -6D, -6D)$ and $(6D, 6D, 6D)$. The cubic surface, where the probes are distributed, is large enough to retain the source's directivity (Bilbao, 2017). To avoid any interpolation procedure, we computed the FW-H acoustic pressure exactly at the grid nodes of the FDTD mesh. The FW-H signal is limited to a period of $T = 0.8\,s$, which corresponds to about 12 revolutions, due to the Large-Eddy Simulation computational cost. In order to make it suitable for the FDTD solver, it is extended from $T = 0.8\,s$ to $T = 3.2\,s$. The FDTD method requires a longer signal since the acoustic field needs to reach a statistically steady state before computing the p_{rms}, where p_{rms} is root-mean-square of the acoustic pressure p. The minimum time required is estimated as the direct acoustic wave's time to reach the farthest boundary. It is easily evaluated since the speed of sound is constant in the domain. The extended signal is obtained by repeating a copy of the FW-H signal, taking care to smoothly paste the signal, the signal being truncated so as not to affect the periodicity (main oscillations are related to the revolution period). The only limitations on this aspect apply to higher frequencies, which may not be in phase when the signal is truncated. However, the frequencies that contain most energy are the lowest; the error in our case can be neglected. All the statistics presented in this paper are collected from $T = 0.8\,s$ to $T = 3.2\,s$.

3 VALIDATION

To check the consistency of the method, we first compared the far-field acoustic pressure resulting from the coupled FW-H-FDTD method with that calculated by FW-H. At this stage we considered open-water conditions: a homogenous infinite domain with $\rho = 998\,Kg/m^3$ and $c = 1400\,m/s$. The FDTD domain is a squared box, $400\,m$ large. At all boundaries, open boundary conditions were set, adopting the PML method; thus, the acoustic energy emitted by the source is allowed to exit the domain. As already mentioned, the FDTD domain is made of cubic cells, $1\,m$ side, which constitute the numerical grid over which the wave equation (Eq. 2) is solved. The acoustic pressure is evaluated with the FW-H method at 60 probes, whose position matches the FDTD computational grid. We compare the acoustic pressure computed through the FW-H equation (Eq. 1) with the one obtained by solving the wave equation (Eq. 2). Three hydrophones were placed upstream of the propeller, namely at $(6D, 2D, 2D)$, $(10D, 2D, 2D)$, and $(38D, 2D, 2D)$. Since only the FW-H linear part has been considered, the problem is rather symmetrical with respect to the upstream/downstream direction and with respect to the azimuth angle (rotation around the propeller axis). In Fig. 1 we show the Spectrum Level (SL) of the acoustic signals, comparing the two methods along with the three probes. The Spectrum Level is evaluated as $SL = 20\log_{10}(A/p_{ref})$, where A is the amplitude of the Fourier transform signal and $p_{ref} = 1\mu Pa$. At the first point, located at $x = 6D$, the spectrum of the two signals coincides, which is expected since the acoustic signal calculated with the FW-H method is imposed as a hard source in the FDTD method. This point highlights that the acoustic noise identified with the FW-H method is used as an imposed boundary condition for the FDTD method. The signals related to the second point $(10D, 2D, 2D)$ show a small discrepancy term of amplitude, which is probably related to the use of the hard source method. We note that $(10D, 2D, 2D)$ is the first point

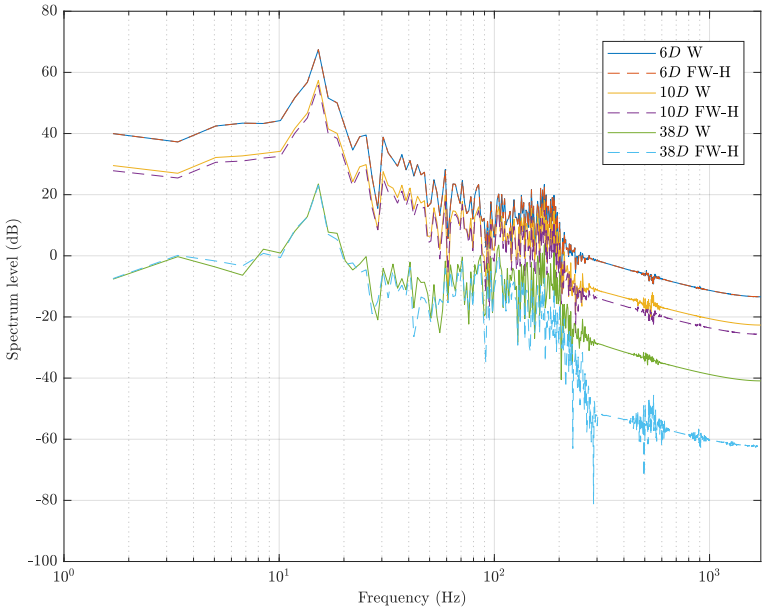

Figure 1. Spectrum Level of the SVA VP1304 marine propeller evaluated with the FW-H (FW-H) method and the FDTD method (W) at three different locations ($6D$, $2D$, $2D$), ($10D$, $2D$, $2D$) and ($38D$, $2D$, $2D$).

in the FDTD computational grid, close to the boundary where we impose the FW-H pressure. A good agreement between the two methods is observed far from the source, at the last point ($38D$, $2D$, $2D$). The amplitude of the two signals is comparable up to $150\,Hz$. At higher frequencies, discrepancies arise, mainly due to the limitation of the wave equation method. We may note that the FDTD method is not able to propagate high-frequency signals at the correct phase velocity. However, since most of the acoustic energy generated from a propeller is concentrated in a low-frequency range, the FDTD method (Eq. 2) can be suitable for our purpose. The advantage of the FDTD method is the ability to generate a three-dimensional acoustic field, enabling a better visualization of its characteristics. As an example we show in Fig. 2 the contour of Sound Pressure Level (SPL) generated by the FDTD solver. The SPL is evaluated as $SPL = 20\log_{10}(p_{rms}/p_{ref})$, where p_{rms} is root-mean-square of the acoustic pressure p and $p_{ref} = 1\mu Pa$.

In the Figure, the x-z plane passing through $y = 2D$ is depicted, considering that the propeller is oriented so as to have the shaft along the x-axis (at $y = z = 0$). As expected, the SPL distribution shows a three-dimensional dipole-like pattern, which, for symmetry reasons, has zero-pressure on the propeller axis. The propeller's dimension (model scale propeller) limits the intensity of the source. In this computational domain the signal reaches the pressure reference p_{ref} soon, giving zero dB signal.

4 RESULTS

In this section, the FDTD method is employed to evaluate the SPL, generated by the propeller, in a confined domain. The FDTD method's enables a better representation of a complex environment; in the present study we propose a domain that is still rather basic, but which shows some interesting differences with respect to the open-space case. We intend to add complexity to the problem, considering more realistic situations, in future works. The domain herein considered is a simplified canal. The canal's depth is $50\,m$, its width is $101\,m$, and it is considered infinite in length, thus open-boundary condition are imposed, making the numerical domain $401\,m$ long. Constant density and speed of sound are considered, set to $\rho = 998\,Kg/m^3$ and $c = 1400\,m/s$, respectively. The source and the nesting procedure are the same as described in the previous section, except for the fact that the propeller is now located at the centre of the canal, at a depth of $4.5\,m$. The boundary conditions now considered, applied to the FDTD numerical domain, substantially modify the acoustic field. The

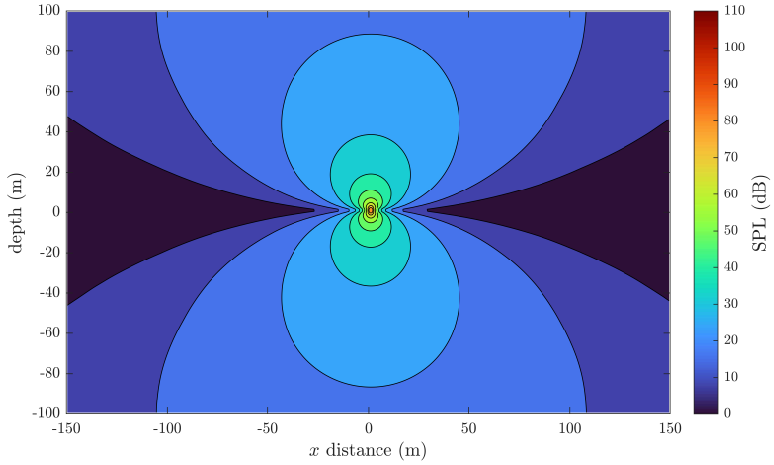

Figure 2. Contour of the SPL on the x-z plane passing through the source at $y = 2D$.

interface between water and air, at $z = 0$ m, is considered as a pressure-free boundary condition. At the bottom of the canal, $z = 50\,m$, a smooth boundary reflects the acoustic energy. Two perfectly reflecting walls are also placed as lateral boundaries, at $y = -50.5\,m$ and $y = 50.5\,m$, being the sides of the canal. A Neumann boundary condition is applied to ensure that all the energy is reflected in the domain. Although this is a simplification, it can be considered an approximation of very dense material, compared to water. All the results related to the canal case are compared with the open-water case, in order to evaluate and highlight differences between the two cases. In Figs. 3, 4, 5, and 6 we show the SPL along different planes for both, the open-water and the canal case. In all Figures, a piece-wise scale of the SPL has been chosen to better visualize the SPL level. The drawback is that the continuous change across two SPL levels is perceived as a chromatic scale variation. In Fig. 3 we show the contour of the SPL on the x-z plane, at $y = 2D$, passing through the source. The x-z plane is parallel to the propeller's motion, and the wake of the propeller develops in the negative x-direction. The SPL patterns in both cases are similar to a dipole field. In the canal case, the acoustic energy

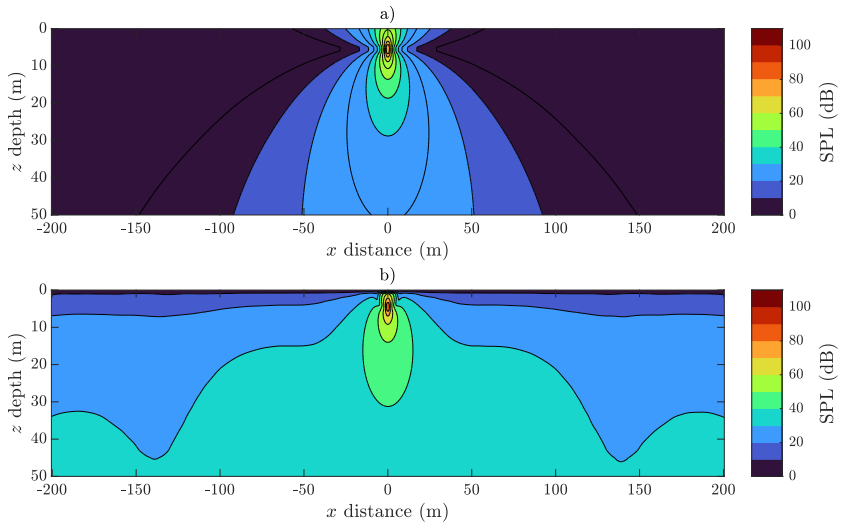

Figure 3. Contour of SPL on the x-z plane passing through the source: *a*) open-sea case, *b*) canal case.

level is strongly affected by the presence of the free surface. A shadow zone is observed, as expected, near the surface $z = 0$, and a higher noise level is observed near the bottom $z = 50\,m$. The walls constrain the acoustic energy inside the domain, and as a result, the noise level increases with respect to the open-water case. The SPL pattern also changes along the width of the canal, as shown in Fig. 4, where the contour of SPL on the y-z, at $x = 2D$, is shown. The y-z plane is parallel to the propeller plane. The decay of the signal, in the open-water case is similar to a monopole. The same

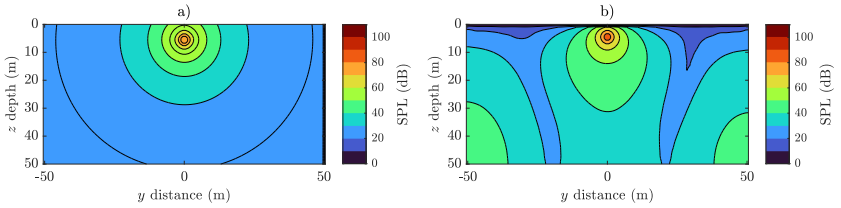

Figure 4. Contour of SPL on the y-z plane passing through the source: *a*) open-sea case, *b*) canal case.

decay is observed in the near field of the canal case, but the overall SPL pattern is strongly affected by the presence of the walls. A low-level zone ($20 - 30\,dB$) is observed approximately halfway from the source, in the y-direction, (see Fig. 4b), which extends from the free surface to the bottom. At the bottom corners of the canal, an increase of the noise level is observed. The SPL pattern is found to be not perfectly symmetric with respect to the centre of the canal. This aspect is related to the interaction between the source and the free-surface, since this asymmetry is not observed in the open-water case. More attention has to be put in the future, on this aspect. The main feature observed on the y-z plane is the presence of constructive/destructive interference zones; indeed, the SPL level varies both with the depth and with distance (along y) from the source. We note that, measuring the noise generated by a propeller in this archetypal environment is not free from uncertainty, since a small difference in the hydrophone position can alter the noise level recorded. The dipole pattern of the SPL level is clear in the x-y plane (Fig. 5), both in the open water case (left panel) and near the source for the canal case (right panel). The positive and negative interference zones are not recognized in the x-y plane depicted in Figure 5, which is the x-y plane, located at $z = 2D$, thus a plane passing through the source; but they are evident at a different depth, $z = 25\,m$, as shown in Fig. 6b. Also in this case, small discrepancies between the two lateral sides, $y = 50\,m$ and $y = -50\,m$, are observed, which makes the SPL distribution asymmetric. The presence of a three-dimensional environment

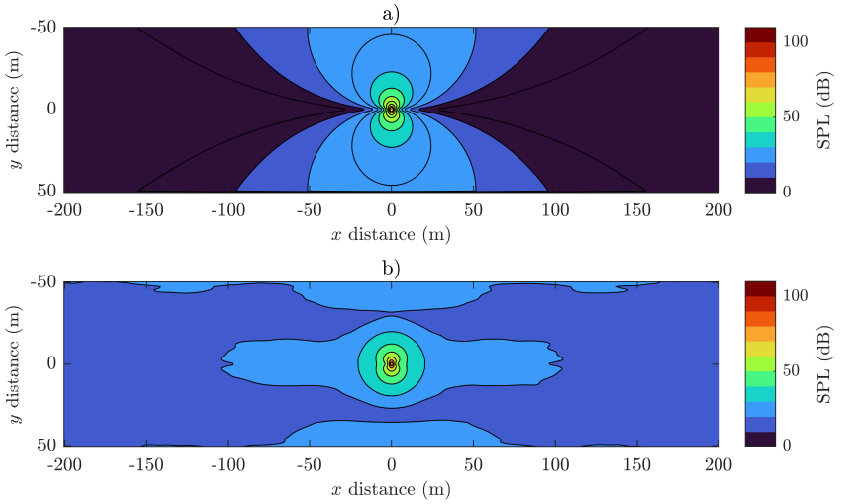

Figure 5. Contour of SPL on the x-y plane passing through the source: *a*) open-sea case, *b*) canal case.

can greatly affect energy propagation along the channel. Compared to the open water case (Fig. 6a), the noise can propagate further along the canal, because of the presence of the wall. This is better depicted in Fig.7, where the SPL is plotted along the x-direction, at $y = 50\,m$, $z = 4.5\,m$ (Figure 7 (a)) corresponding to the source depth, and at $y = 50\,m$, $z = 25\,m$ (Fig. 7b). The continuous line corresponds to the open water case, and the dotted line to the canal case. The main remark in Fig. 7a is the different decay in the near field. In the open water case the decay is spherical, because of the unbounded domain. In the canal case, three different zones with diverse decay rates are observed. In the first zone, near the source, the acoustic pressure has a spherical decay up to the free surface, namely the boundary first met by the signal. After that the free surface reflects the acoustic pressure, the decay becomes cylindrical (second zone). The third zone is then observed after approximately

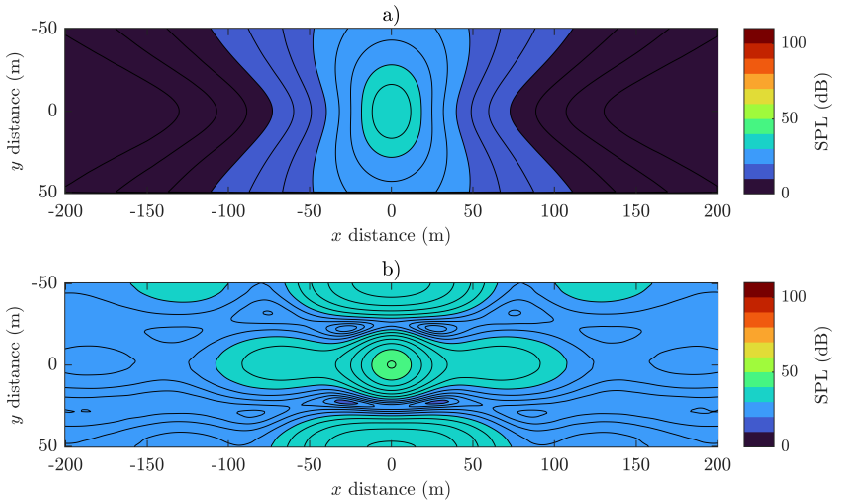

Figure 6. Contour of SPL on the x-y plane at the depth of $z = 25\,m$: a) open-sea case, b) canal case.

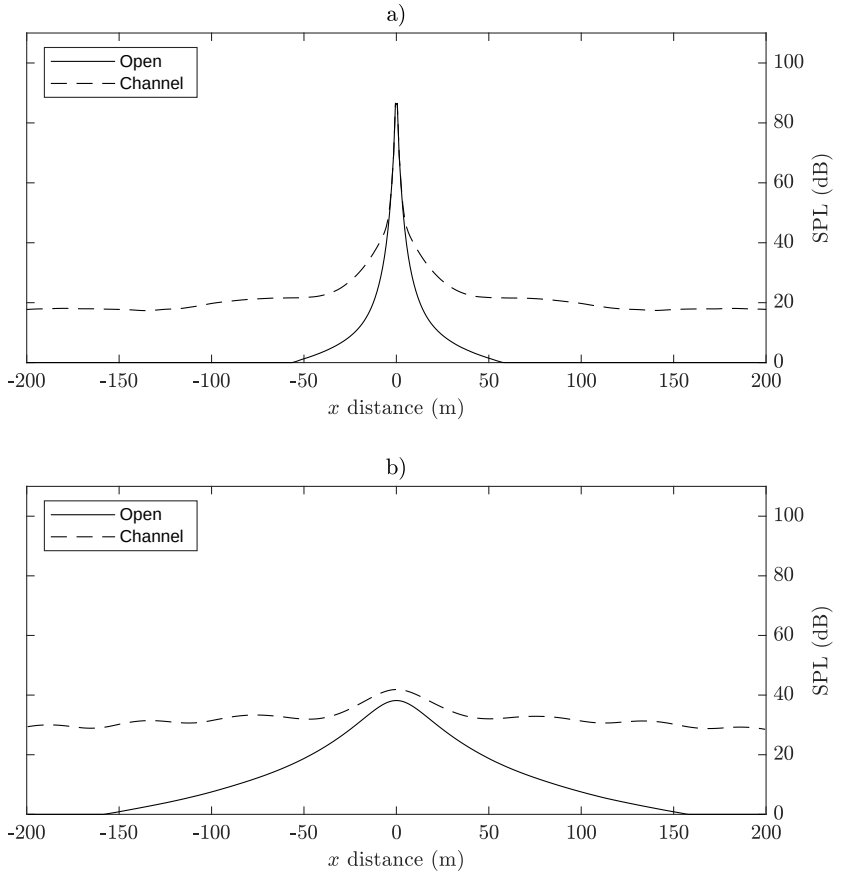

Figure 7. SPL on the x-z line: a) passing through the source, b) at the depth of $z = 25\,m$.

$50\,m$ when the acoustic waves reach the canal's lateral wall, and the decay is constant. A difference of about $20\,dB$ between the two cases is observed. Moreover, the difference between the open-water case and the canal case increases with depth, as shown in Fig. 7b. At this depth, the difference reaches $25\,dB$. As noted before, the SPL distribution also changes in the y-direction, which is the direction perpendicular to the motion, but maintaining almost symmetric behaviour with respect to the canal's centre. This is highlighted in Fig. 8, where we plot the SPL along a line in the y-z plane, at $z = 4.5\,m$ (8a), and at $z = 45\,m$ (8b). In particular, in Fig. 8a, the decay of the SPL level in the canal case is altered by the wall, compared to the open water case. The negative interference zone is visible at the half-width of the canal, at about $y = \pm 25\,m$. In Fig. 8b, the SPL measured in the canal case

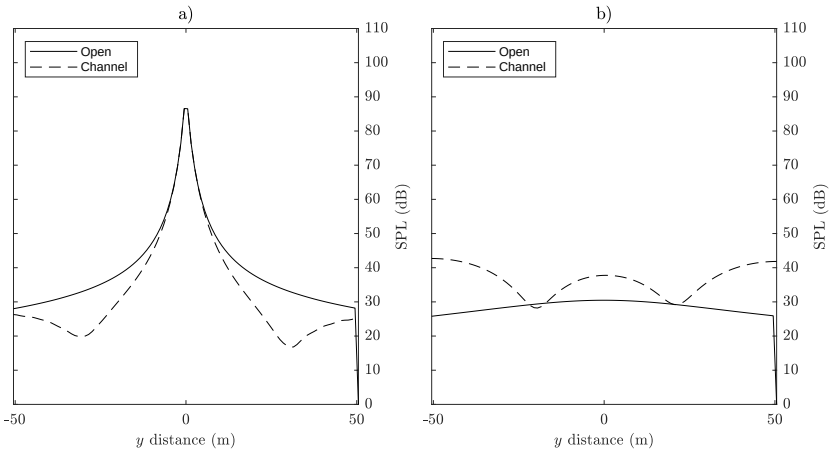

Figure 8. SPL on the x-z line: a) passing through the source, b) at the depth of $z = 25\,m$.

is greater than that of the open water case, as expected, and the positive and negative interference zone is observed. A strong variability of the SPL is observed along the width and the depth of the canal. Moreover, what we noticed so far is that the SPL patterns, thus the environment response to a specific source, changes according to several features, such as: the source's position, the source signal, and the ratio between the canal's dimensions and the main wavelengths associated to the source.

5 CONCLUSIONS

In the present work, we have developed a numerical method based on coupling two well-established methodologies, namely the Ffowcs-Williams and Hawkings acoustic analogy and numerical solution of the wave equation using the Finite Difference Time Domain method. The former is used to characterize the source, in this case, a marine propeller, and to provide the acoustic signal at several probes; the latter uses the signal at the probes as imposed boundary conditions and propagates the pressure disturbance in an arbitrary domain. This method allows quantifying how complex noise sources propagate in non-homogeneous and bounded domains. As a preliminary study, we considered two simple domains for the FDTD solver: an open domain (which made the results comparable to the free-space solution of FW-H) and a canal, which highlight the importance of reflecting boundaries. Differences in the acoustic field between the two configurations are visible and encourage a more detailed study, both as regards the FW-H part (we will consider the contribution of the wake as a noise source, which was neglected in the present work) and, mostly, regarding the complexity of the FTDT domain.

REFERENCES

Bensow, R., and Liefvendahl, M. (2016). An Acoustic Analogy and Scale-Resolving Flow Simulation Methodology for the Prediction of Propeller Radiated Noise. *31th Symposium on Naval Hydrodynamics*, September 11, Monterey, CA, USA.

Bilbao, S. and Hamilton, B. (2017). Directional source modeling in wave-based room acoustics simulation. *IIEEE Workshop on Applications of Signal Processing to Audio and Acoustics (WASPAA)*, October 15-18, New Paltz, NY, USA.

Broglia, R., Cianferra, M., Posa,A., Felli, M., and Armenio, V. (2020). Hydroacoustic Analysis of a Marine Propeller in Open Water Conditions through LES and Acoustic Analogy. *33rd Symposium on*

Naval Hydrodynamics. October 18-23, Osaka, Japan.

Chern, A. (2019). A Reflectionless Discrete Perfectly Matched Layer. *Journal of Computational Physics*, 381, 91-109.

Cianferra, M., Petronio, A., and Armenio, V. (2019). Non-Linear Noise from a Ship Propeller in Open Sea Condition. *Ocean Engineering*, 191, 106474.

Etter, P. C. (2012), Advanced Applications for Underwater Acoustic Modeling. *Advances in Acoustics and Vibration* .

Hildebrand, John A. (2009). Anthropogenic and Natural Sources of Ambient Noise in the Ocean. *Marine Ecology Progress Series*, 395, 5-20.

IMO, M. (2014). Guidelines for the reduction of underwater noise from commercial shipping to address adverse impacts on marine life. MEPC.

Felli, M., Grizzi, S., and Falchi, M. (2014). A Novel Approach for the Isolation of the Sound and Pseudo-Sound Contributions from Near-Field Pressure Fluctuation Measurements: Analysis of the Hydroacoustic and Hydrodynamic Perturbation in a Propeller-Rudder System. *Experiments in fluids*, 55.1, 1-17.

Hafla, E., Johnson, E., Johnson, C. N., Preston, L., Aldridge, D., and Roberts, J. D. (2018). Modeling Underwater Noise Propagation from Marine Hydrokinetic Power Devices through a Time-domain, Velocity-Pressure Solution. *The Journal of the Acoustical Society of America*, 143.6, 3242-3253.

Ianniello, S., Muscari, R., and Di Mascio, A. (2014). Ship Underwater Noise Assessment by the Acoustic Analogy Part II: Hydroacoustic Analysis of a Ship Scaled Model. *Journal of marine Science and technology*, 19.1, 52-74.

Keller, J., Kumar, P., and Mahesh, K. (2018). Examination of Propeller Sound Production Using Large Eddy Simulation. *Physical Review Fluids*, 3.6, 064601.

McKenna, M. F., Ross, D., Wiggins, S. M., and Hildebrand, J. A. (2012). Underwater Radiated Noise from Modern Commercial Ships. *The Journal of the Acoustical Society of America*, 131.1, 92-103.

Sturm, F. (2005). Numerical Study of Broadband Sound Pulse Propagation in Three-Dimensional Oceanic Waveguides. *The Journal of the Acoustical Society of America*, 117.3, 1058-1079.

Weilgart, L. S. (2007). A Brief Review of Known Effects of Noise on Marine Mammals. *International Journal of Comparative Psychology*, 20(2).